Journal for ImmunoTherapy of Cancer

CXCR6 deficiency impairs cancer vaccine efficacy and CD8$^+$ resident memory T-cell recruitment in head and neck and lung tumors

Soumaya Karaki,[1,2] Charlotte Blanc,[1,2] Thi Tran,[1,2] Isabelle Galy-Fauroux,[1,2] Alice Mougel,[1,2] Estelle Dransart,[3] Marie Anson,[1,2] Corinne Tanchot,[1,2] Lea Paolini,[1,2] Nadege Gruel,[4,5] Laure Gibault,[6] Francoise Lepimpec-Barhes,[7] Elizabeth Fabre,[8] Nadine Benhamouda,[9] Cecile Badoual,[6] Diane Damotte,[10] Emmanuel Donnadieu ,[11] Sebastian Kobold,[12,13] Fathia Mami-Chouaib,[14] Rachel Golub,[15] Ludger Johannes,[3] Eric Tartour [1,2,9]

To cite: Karaki S, Blanc C, Tran T, *et al*. CXCR6 deficiency impairs cancer vaccine efficacy and CD8$^+$ resident memory T-cell recruitment in head and neck and lung tumors. *Journal for ImmunoTherapy of Cancer* 2021;**9**:e001948. doi:10.1136/jitc-2020-001948

► Additional material is published online only. To view, please visit the journal online (http://dx.doi.org/10.1136/jitc-2020-001948).

SK, CB and TT contributed equally.

RG, LJ and ET are joint senior authors.

Accepted 24 January 2021

For numbered affiliations see end of article.

Correspondence to
Professor Eric Tartour;
eric.tartour@aphp.fr

ABSTRACT

Background Resident memory T lymphocytes (T_{RM}) are located in tissues and play an important role in immunosurveillance against tumors. The presence of T_{RM} prior to treatment or their induction is associated to the response to anti-Programmed cell death protein 1 (PD-1)/Programmed death-ligand 1 (PD-L1) immunotherapy and the efficacy of cancer vaccines. Previous work by our group and others has shown that the intranasal route of vaccination allows more efficient induction of these cells in head and neck and lung mucosa, resulting in better tumor protection. The mechanisms of in vivo migration of these cells remains largely unknown, apart from the fact that they express the chemokine receptor CXCR6.

Methods We used *CXCR6*-deficient mice and an intranasal tumor vaccination model targeting the Human Papillomavirus (HPV) E7 protein expressed by the TC-1 lung cancer epithelial cell line. The role of CXCR6 and its ligand, CXCL16, was analyzed using multiparametric cytometric techniques and Luminex assays.
Human biopsies obtained from patients with lung cancer were also included in this study.

Results We showed that CXCR6 was preferentially expressed by CD8$^+$ T_{RM} after vaccination in mice and also on intratumoral CD8$^+$ T_{RM} derived from human lung cancer. We also demonstrate that vaccination of Cxcr6-deficient mice induces a defect in the lung recruitment of antigen-specific CD8$^+$ T cells, preferentially in the T_{RM} subsets. In addition, we found that intranasal vaccination with a cancer vaccine is less effective in these *Cxcr6*-deficient mice compared with wild-type mice, and this loss of efficacy is associated with decreased recruitment of local antitumor CD8$^+$ T_{RM}. Interestingly, intranasal, but not intramuscular vaccination induced higher and more sustained concentrations of CXCL16, compared with other chemokines, in the bronchoalveolar lavage fluid and pulmonary parenchyma.

Conclusions This work demonstrates the in vivo role of CXCR6-CXCL16 axis in the migration of CD8$^+$ resident memory T cells in lung mucosa after vaccination, resulting in the control of tumor growth. This work reinforces and explains why the intranasal route of vaccination is the most appropriate strategy for inducing these cells in the head and neck and pulmonary mucosa, which remains a major objective to overcome resistance to anti-PD-1/PD-L1, especially in cold tumors.

INTRODUCTION

Different subpopulations of memory CD8$^+$ T cells have been characterized: (1) central memory CD8$^+$ T cells, expressing CCR7 and CD62L lymph node-homing receptors, are mainly found in secondary lymphoid organs; (2) effector-memory CD8$^+$ T cells, not expressing the receptors for migration to lymphoid organs, circulate in the periphery and in tissues and play an effector role (ie, release of cytotoxic granules and cytokine secretion); (3) CD8$^+$ memory stem cells are poorly differentiated with a high capacity for self-renewal and proliferation and are able to reconstitute the whole spectrum of memory CD8$^+$ T-cell populations; and (4) resident memory CD8$^+$ T cells (T_{RM}) expressing retention receptors such as CD103, CD49a and CD69, are found in non-lymphoid peripheral tissues and do not recirculate except for possible retrograde transport in lymph nodes.[1] Recent studies have also reported that CD8$^+$ T_{RM} cells can give rise to circulating effector and memory T cells, but they remain predisposed to migrate back to their tissue of origin.[2] These cells are among the first cells able to act in healthy or tumor tissues, and because of their local mobility, they play a major role in tissue immune surveillance.[3 4] After their activation, these cells also allow the recruitment of circulating immune cells via the secretion of cytokines and chemokines

in order to amplify the local immune response.[5] These T_{RM} cells appear to be more cytotoxic than other $CD8^+$ T effector cells, as CD103 expression is correlated with the levels of granzymes.[6]

The role of T_{RM} in antitumor immunity has recently been highlighted. For example, it has been shown in mice that these lymphocytes delay tumor progression.[7 8] Our team has shown that T_{RM} specifically induced by intranasal vaccination plays an essential role in controlling the growth of orthotopic murine head and neck or lung tumors.[9 10] Other studies have identified T_{RM} as a key mediator of cancer vaccines targeting mucosal tumors.[11 12]

In humans, T_{RM} has been found in different types of cancer, such as melanoma, urothelial carcinoma, endometrial adenocarcinoma, and particularly lung cancer.[9 13 14]

Our team and other groups have shown that a larger $CD103^+CD8^+$ T-cell infiltrate was associated with better survival in lung cancer, even in multivariate analysis.[6 9 13] In the present study, we wanted to analyze the mechanism by which intranasal vaccination promotes preferential intratumoral infiltration of T_{RM} in head and neck cancer and lung tumors, compared with systemic vaccination. Previous results, based on phenotypical and transcriptomic analysis, from our team and other groups, have identified CXCR6 chemokine receptor as a core marker of T_{RM} present in lung or head and neck tumors, but its function has not been investigated.[6 9 15–18]

CXCR6 binds a unique ligand, CXCL16, which can exist in transmembrane and soluble forms,[19] the latter requiring cleavage from the membrane by a disintegrin and metalloproteinase domain-10, or a disintegrin and metalloproteinase domain-17.[20] CXCL16 is produced by epithelial and immune cells and can serve as an alarmin to recruit cells to the site of inflammation.[21 22]

In contrast with T_{RM}, CXCR6 is detected at very low levels on naive $CD8^+$ T cells[19] and is upregulated by priming by dendritic cells,[23] or after T-cell receptor activation.[24]

CXCR6 promotes homing of lymphocytes to non-lymphoid tissues, such as the skin,[25] the liver in hepatitis C,[26] the synovium in rheumatoid arthritis[27] and the brain in experimental autoimmune encephalomyelitis.[28]

Cxcr6 is also one of the 100 genes presenting the greatest difference in expression between T_{RM} in the lung and Teff in the blood.[29] The fact that interleukin-15 is required for the differentiation of T_{RM}[30 31] and upregulates the expression of CXCR6[32] reinforces the link between CXCR6 and T_{RM}.

As the role of CXCR6 in the migration of tumor-specific T_{RM} to mucosal cancers (head and neck and lung cancers) after intranasal vaccination has not yet been addressed, we chose in the present work to focus on this key question, as it might have direct consequences on patient response to cancer immunotherapy.

MATERIALS AND METHODS

Mice

Female C57BL/6J wild-type mice were purchased from Janvier Labs. *CXCR6*$^{gfp/gfp}$ mice, are homozygous *CXCR6*-deficient mice, in which the coding region of the chemokine receptor CXCR6 has been substituted with the coding region of the Enhanced Green Fluorescent Protein (eGFP). These mice were obtained from Jackson Laboratory (cat# JAX: 005693) and bred in our animal facility. Male *CXCR6*$^{gfp/gfp}$ mice were crossed with female C57BL/6J mice to generate *CXCR6*$^{gfp/+}$ mice. B6.SJL-*Ptprc*^{a}*Pepc*^{b}*/BoyJ* (CD45.1) were purchased from Charles River. CD3 knockout (KO) mice were obtained from B Malissen's laboratory (CIML, Marseille, France) and bred in our animal facility.

Mice were used in experiments at 8–10 weeks of age. All mice were housed in INSERM U970-PARCC animal facility under specific pathogen-free conditions.

Tumor cells

TC-1 cells expressing the Human Papillomavirus (HPV)16 E6–E7 proteins were obtained from the laboratory of T C Wu (Department of Pathology, School of Medicine, Johns Hopkins University, Baltimore, Maryland, USA). Cells were cultured in RPMI 1640 (Life Technologies) supplemented with 10% heat-inactivated fetal calf serum (FCS, GE Healthcare), 1 mM sodium pyruvate (Life Technologies), 1 mM non-essential amino acids (Life Technologies), 100 U/mL penicillin and 100 µg/mL streptomycin (Life Technologies), and 0.5 mM 2-β mercaptoethanol (Life Technologies), and incubated at 37°C in 5% CO_2. They were regularly tested for mycoplasma contamination.

Vaccine and adjuvant

The STxB-E7 vaccine was produced by the chemical coupling of the N-bromoacetylated $E7_{43–57}$ peptide to the sulfhydryl group of a recombinant nontoxic Shiga toxin B-subunit variant according to previously described procedures.[33] After purification, endotoxin concentrations determined by the Limulus assay test (Lonza, Aubergenville, France) were <0.5 endotoxin unit/mg. Polyinosinic-polycytiylic acid-poly-l-lysine carboxymethylcellulose (Poly-ICLC) were obtained from Oncovir (Washington, USA).

Tumor challenge and vaccination protocol

Anesthetized mice were injected with 5×10^4 TC-1 tumor cells in the submucosal area of the tongue with a Hamilton Gastight syringe of 10 µL, or in the mucosal part of the cheek with a 26 G insulin syringe. Mice were daily monitored for survival analysis, and tumor size was measured every 2–3 days with a caliper (volume mm^3=(length×width×width)/2).

Anesthetized mice were immunized two times per day (D)0 and at D14 by intranasal or intramuscular routes with STxB-E7 (20 µg) associated with poly-ICLC (10 µg) as adjuvant for the first immunization. Total volume injected was 25 µL for the intranasal route and 50 µL for the intramuscular route. In the prophylactic setting, tumors were grafted 7 days after the second immunization, whereas for the therapeutic setting, mice were vaccinated at D5 and

10 after tumor graft for tongue tumor and at D7 and D14 for cheek tumor.

The mean survival time was calculated using the Kaplan–Meier method and statistical analysis was performed using a log-rank test. Analysis of differences in tumor volume were performed with two-way analysis of variance (ANOVA) and Bonferroni or Tukey post hoc test.

Isolation of lymphocytes from bronchoalveolar lumen fluid, lung parenchyma, tumors and spleen

Intravascular staining was performed to discriminate between tissue-localized and blood-borne cells as described by Anderson *et al*.[34] Briefly, 5 µg of anti-CD8a APC-efluo780 (clone 53-6-7, ebioscience/Thermofisher) was injected intravenously 3 min prior to bronchoalveolar lavage (BAL) and tissue harvest.

Bronchoalveolar lavage (BAL) was obtained by flushing the lungs with phosphate-buffered saline (PBS)-EDTA 0.5 mM via a cannula inserted in the trachea (5 washes×1 mL).

Lungs were perfused with PBS-EDTA 0.5 mM and digested in RPMI-1640 medium supplemented with 1 mg/mL collagenase type IV (Life Technologies/Thermofisher) and 30 µg/mL DNase I (Roche). Lungs were dissociated using the GentleMACS (Miltenyi Biotec, France) lung programs 1 and 2, with gentle shaking at 37°C for 30 min in between both steps. Then, the obtained single-cell suspensions were filtered through a 70 µm strainer washed with PBS–FBS 2%, suspended in 40% Percoll solution and layered over 75% Percoll solution (Sigma-Aldrich), and centrifuged at 600×*g* for 20 min at room temperature (RT). Interface cells were collected and washed. Tumors were harvested, minced and placed into GentleMACS C-tube with PBS-FCS 2%, dissociated mechanically with GentleMACS dissociator (Miltenyi) according to the manufactor's standard protocol, then filtered on a 70 µm strainer.

Spleens were dissected and pressed through a 40 µM cell strainer, red blood cells were lysed with osmotic lysis buffer.

Cheek tumors were harvested and mechanically dissociated by using the GentleMACS (Miltenyi, Bergisch Gladbach, Germany) (program m-imp-tumor-01–01), then filtered on a 70 µm strainer.

Flow cytometry

After FcR blocking with CD16/32 Ab (clone 93, ebioscience/ Life Technologies), cells were first incubated for 30 min at RT with PE-conjugated $D^bE7_{49–57}$ (R9F) tetramer (Immudex). Then, cells were washed and stained 20 min at 4°C with the following Abs : anti-mouse CD8b AF700 or BUV495 (clone YTS156), CD3 PercpCy5.5 (clone 145 2C11, ebioscience/Life Technologies), CD103 Pacific Blue (clone 2E7, Biolegend), and CD49a Alexa 647 (clone Ha31/8, BD Biosciences). For chemokine receptor analysis, cells were stained 30 min at RT with anti-mouse CCR5 PE-CY7 (clone HM-CCR5), CCR6 BV785 (clone 29–2 L17), CXCR3 BV650 (clone CXCR3-173), CXCR6 BV711 (clone SA051D1) (all Abs from Biolegend). Then staining was performed as described previously. All the cells were labeled using the live/dead cell aqua blue viability (Life Technologies).

Non-circulating $CD8^+$ T cells were defined as $CD3^+CD8a^{neg}CD8b^+$. Acquisitions were performed on BD Fortessa X20 (Becton Dickinson), and data were analyzed on live singulet cells with FlowJo Software (BD).

Chemokines multiplex assays and ELISA

Supernatants from the first BAL's washes were collected. Serum samples were prepared from blood collected from retro-orbital sinus. Proteins were extracted from perfused lungs and from spleen by using Bioplex lysis buffer (Bio-Rad), and total proteins were determined by bicinchoninic acid (BCA) assay (Pierce) according to the manufacturer's protocol.

Chemokines was measured by bead-based multiplex immunoassay: CXCL16, MIP1a/CCL3,MIP1b/CCL4,RANTES/CCL5,IP10/CXCL10, CCL20 (R&D Systems Biotechne), according to manufacturer protocol and were analyzed on Bio-Plex 200 (Bio-Rad). The analyte concentration was calculated using a standard curve (5 Parameter logistic (PL) regression), with Bio-Plex manager software. When indicated, CXCL16 was measured by ELISA (R&D Systems Biotechne) according to manufacturer protocol.

Transcriptomic analysis

C57BL/6 mice were immunized with STxB-E7 (20 µg)+α-GalCer (2 µg) by intranasal or intramuscular route and then immunized a second time with STxB-E7 (20 µg) 14 days later (prime-boost). Seven days after the second immunization, the BAL or spleen of the mice were recovered, and the $CD44^{hi}tetramer^+CD8^+T$ cells were sorted by BD FACSAria II cell sorter. Then, RNA of the cells was extracted using the QIAGEN RNeasy Plus Micro Kit and then genotyped by DNA chip (Affymetrix) by the genomics and transcriptomics platform of the Cochin Institute.

Data were normalized using Robust Multiarray Averaging (RMA) algorithm in Bioconductor with the custom CDF vs 18 (Dai M et al Nucleic Acids Res 2005). Statistical analysis was carried out with the use of Partek GS. All the data have been deposited in NCBI's Gene Expression Omnibus44 and are accessible through GEO Series accession number GSE77366 (http://www.ncbi.nlm.nih.gov/geo/query/acc.cgi?token=ghsrcweibruzvsj&acc=GSE77366).

First, variations in gene expression were analyzed using unsupervised hierarchical clustering and PCA to assess data from technical bias and outlier samples. To find differentially expressed genes, we applied one-way ANOVA for each gene and made pairwise Tukey's post hoc tests between groups. Then, we used p values and fold changes to filter and select differentially expressed genes. Differentially expressed genes (DEG) enrichment

analysis was carried out using Ingenuity (Ingenuity Systems, USA; www.ingenuity.com).

Data availability

All data were deposited in NCBI's Gene Expression Omnibus and are accessible through GEO Series accession number GSE77366 (http://www.ncbi.nlm.nih.gov/geo/query/acc.cgi?token=ghsrcweibruzvsj&acc=GSE77366).

Human lung cancer

Lung cancer biopsies were obtained from non-treated patients with non-small-cell lung carcinoma who underwent a lobectomy at the thoracic surgery department of European Georges Pompidou Hospital. Briefly, biopsies were digested for 45 min at 37°C with DNAse I (30 IU/mL, Roche) and collagenase type IV (1 mg/mL, Life Technologies/Thermofisher), then filtered through a 70 µm strainer washed with PBS–FCS 2%. Flow cytometry analysis of tumor-infiltrating lymphocytes was performed. : Receptors for the Fc region (FcRs) were first blocked with Human TruStain FcX (Biolegend) 5 min at RT, then stained with anti-human CD3 APC-CY7 (clone HIT-3a, Biolegend), CD8 BUV395 (clone RPA-T8, BD Biosciences), CD103 Percpcy5.5 (clone Ber-ACT8, Biolegend), CD49a PE (clone TS2-7, Biolegend), PD1 BV650 (clone EH12.2H7, Biolegend), CXCR6 biotin (clone K041E5, Biolegend) and steptavidin BV711 (Biolegend). All cells were labeled using the live/dead cell aqua blue viability (Life Technologies). Acquisitions were performed on BD Fortessa X20 (Becton Dickinson), and data were analyzed on live singulet cells with FlowJo Software (BD).

Statistical analysis

Data are presented as mean±SEM. Statistical comparisons were done with Prism V.8 GraphPad Software (San Diego, California, USA). Analysis of difference between two groups was performed with Mann-Whitney t-test; analysis of difference between more than two groups was performed with a one-way ANOVA and Holm-Sidak or Tukey post hoc. Mice survival was estimated using the Kaplan-Meier method and log-rank test. P values lower than 0.05 (*) were considered significant.

RESULTS

CXCR6 expression is upregulated on CD8$^+$ T cells with a T_{RM} phenotype induced by ntranasal vaccination

Our previous study showed that in contrast to the spleen-derived $E7_{39–47}$-specific CD8$^+$ T cells induced by intramuscular immunization, the BAL's $E7_{49-57}$-specific CD8$^+$ T cells induced by intranasal immunization express the core gene defining T_{RM} (Itgae encoding CD103, Itga1 encoding CD49a and Itgb1, which associates with Itga1 to form the VLA-1 integrin).[9] Here, we have completed this analysis by a transcriptomic analysis, showing that $E7_{49–57}$-specific CD8$^+$ T cells with induced by intranasal immunization in the BAL and displaying a T_{RM} phenotype preferentially

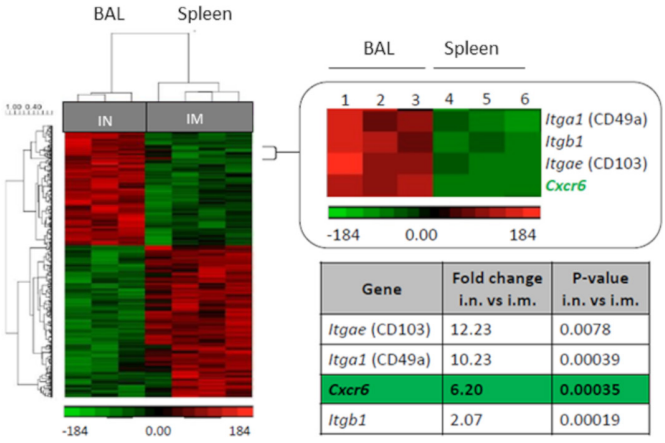

Gene	Fold change i.n. vs i.m.	P-value i.n. vs i.m.
Itgae (CD103)	12.23	0.0078
Itga1 (CD49a)	10.23	0.00039
Cxcr6	6.20	0.00035
Itgb1	2.07	0.00019

Figure 1 Cxcr6 upregulation on CD8$^+$ T cells with a T_{RM} phenotype induced by intranasal vaccination revealed by heat MAP analysis. Mice were vaccinated via intranasal or intramuscular routes (n=4 mice per group) with STxB-E7 and the adjuvant α-GalCer (prime D0) and boosted at D14 with STxB-E7. BAL from in vaccinated mice and spleens from intramuscularly vaccinated mice were collected at day 21. H2-D^b $E7_{49-57}$ tetramer$^+$ CD44^{hi} CD8$^+$ T cells were sorted and the RNA was extracted. Whole gene expression microarray analysis was performed according to the procedure described in the methods section. Left: total gene analysis already reported in Nizard *et al*[9] and not detailed here. Right: focus on the expression of CXCR6 by T_{RM} cells. Top: BAL CD8$^+$ T cells (lanes 1–3) showed a typical T_{RM} gene expression profile (CD103$^+$ and CD49a$^+$), which was not observed in splenic CD8$^+$ T cells (lanes 4–6) (red square means overexpressed, while green square means underexpressed). Bottom: table of the transcriptomic characteristics of the *Itga1*, *Itgb1*, *Itgae* and *Cxcr6* RNAs, with their p value and 'fold change'. The fold change represents the difference in quantity between the genes expressed by CD8$^+$ T cells from BAL after intranasal immunization and from the spleen after intramuscular immunization. These extractions were repeated at least three times. BAL, bronchoalveolar lavage.

express CXCR6 compared with those induced in the spleen after intramuscular immunization (fold change 6.2, p=0.00035) (figure 1, right). As we have previously reported, intramuscular vaccination did not induce T_{RM} in the BAL and we could not check for their expression of CXCR6 after this route of immunization.[9]

CXCR6 is preferentially expressed on intranasal vaccine-induced E7-specific CD8$^+$ T cells displaying resident memory T cell (T_{RM}) phenotype

To investigate the potential role of CXCR6 in the establishment of lung-homing CD8$^+$ T-cell populations, we used heterozygous *Cxcr6* $^{gfp/+}$ mice, in which one allele of the Cxcr6 gene has been replaced by the coding region of *gfp*.[35] We also examined the expression of CXCR6 on lung resident CD8$^+$ T cells at the protein levels using a recently available anti-CXCR6 antibody. In the first series of experiments, *Cxcr6*$^{gfp/+}$ mice were first grafted with TC-1 cells in the tongue, then intranasally immunized with STxB-E7 at D5 and D10, and then tumor, BAL, lung and spleen

were harvested at D15 (figure 2A). We then analyzed CXCR6 expression on $E7_{49-57}$-specific $CD8^+$ T cells with a T_{RM} phenotype, defined as $CD8^+$ T cells expressing CD103 and/ or CD49a as previously reported,[9] or with an effector phenotype without the expression of these markers. CXCR6 was analyzed by flow cytometry based on GFP expression or with the use of anti-CXCR6 mAb (figure 2B).[9] In tumor, lung parenchyma and BAL, we found a statistically significant increase in membrane CXCR6 expression on E7-specific $CD8^+$ T cells with a T_{RM} phenotype, when compared with cells with an effector phenotype (figure 2C).

Surprisingly no difference in the expression of GFP could be detected between the T_{RM} and the effector T cells in the various organs (online supplemental figure S1). Differences in the expression of GFP and membrane CXCR6 had already been observed with these mice.[36] We considered that the membrane expression of CXCR6 was the most relevant cellular localization for the function of a chemokine receptor.

Next, we validated this preferential expression of CXCR6 on human T_{RM} derived from lung tumors. Remarkably, 58% of intratumoral T_{RM} expressed CXCR6, while it is detected on only 20% of intratumoral effector $CD8^+$ T cells (figure 2D,E). CXCR6 Mean fluorescence intensity (MFI) expression was also higher on T_{RM} than on effector cells (figure 2E). Phenotype characterization of these $CXCR6^+$ T_{RM} showed that they express PD-1 more strongly than CXCR6 negative T_{RM} (figure 2F). These results show that both mouse and human tumor T_{RM} cells preferentially expressed CXCR6 compared with effector T cells.

CXCR6 deficiency impairs induction of antigen-specific $CD8^+$ T cells and T_{RM} in the airway after intranasal vaccination

We then investigated the role of CXCR6 in the induction of $E7_{49-57}$-specific $CD8^+$ T and T_{RM} cells in BAL and spleen using mice lacking this chemokine receptor (*Cxcr6*$^{gfp/gfp}$) (figure 3A). We observed a statistically significant reduction in the total number of $E7_{49-57}$-specific $CD8^+$ T and T_{RM} cells in BAL and lung parenchyma of *Cxcr6*-deficient mice, when compared with C57BL/6 wild-type mice (figure 3B,C). This decrease is more pronounced on E7 specific T cells with a T_{RM} phenotype than with an effector phenotype (figure 3D). The latter population is even increased in *Cxcr6*-deficient mice compared with wild-type mice (figure 3D). After vaccination, we did not find any difference in the $E7_{49-57}$ tetramer levels in the spleen between wild-type and *Cxcr6*$^{gfg/gfp}$mice (online supplemental figure S2A,B). Notably, CXCR6 membrane expression on $E7_{49-57}$ specific $CD8^+$ T cells was not detected in the spleen of *Cxcr6*$^{gfp/+}$ mice (online supplemental figure S2C).

As *Cxcr6* deficiency is not restricted to T cells only, we performed a transfer experiment, in *CD3*-deficient mice, with T cells derived from wild-type mice (CD45.1) or *Cxcr6*-deficient mice (CD45.2). We show that mice which had received the *Cxcr6*-deficient T cells had a decrease in the absolute number of anti-$E7_{49-57}$ $CD8^+$ T cells in the BAL compared with mice which had received T cells derived from wild-type mice. A similar trend exists in the pulmonary parenchyma. This result confirms the intrinsic role of *Cxcr6* deficiency in T cells on the decrease of the local T_{RM} after vaccination by the intranasal route (online supplemental figure S3).

CXCR6 deficiency partially reverses cancer vaccine control of tumor growth in orthotopic head and neck tumor models

To assess the consequence of *Cxcr6* deficiency on the recruitment of $CD8^+$ T cells in the tumor microenvironment and on the control of tumor growth, we set up two orthotopic models using TC-1 tumor cells that were grafted in the cheek or in the tongue.

C57BL/6 wild-type or *Cxcr6* $^{gfp/gfp}$ mice were challenged with TC-1 cells in the submucosal lining of the cheek (intracheek) then vaccinated or not with STxB-E7 by intranasal route at D7 and D14, and the tumor volume was monitored (figure 4A). Vaccinated C57BL/6 wild-type mice showed significant inhibition of tumor growth based on the measurement of tumor weight or tumor size in comparison to non-vaccinated mice (figure 4B–D). In contrast, we observed a partial loss of tumor control by the vaccine in *Cxcr6* $^{gfp/gfp}$ mice (figure 4B–D).

To confirm these results in a second orthotopic tumor model, C57BL/6 wild-type mice and *Cxcr6*$^{gfp/gfp}$ mice were engrafted in the sublingual mucosa with TC-1 cells and were vaccinated prophylactically (before the graft) (figure 4E) or therapeutically (after the graft) (figure 4F) with STxB-E7 by intranasal route.

In both settings, all vaccinated C57BL/6 wild-type mice were alive at D60 for the prophylactic model (figure 4E) and at D25 for the therapeutic model (figure 4F). In *Cxcr6*$^{gfp/gfp}$, only 60% of vaccinated mice were alive in both models at the same time points. Survival curves indicate that vaccinated *Cxcr6*$^{gfp/gfp}$ mice showed decreased survival compared with vaccinated C57BL/6 wild-type mice. These results indicate that impairment of CXCR6 expression has a strong negative impact on antitumor immunity.

We then addressed whether this partial loss of tumor growth control after vaccination is associated with a reduction of intratumoral infiltration by $CD8^+$ T cells. Tumor-infiltrating lymphocytes were analyzed by flow cytometry in C57BL/6 wild-type or *Cxcr6g*$^{gfp/gfp}$ mice engrafted with TC-1 tumor cells in the submucosal lining of the cheek, and vaccinated or not with STxB-E7 at D7 and D14. A significant decrease in the absolute numbers of intratumoral $CD8^+$ T cells, total $H\text{-}2D^b\text{-}E7_{49-57}$ $CD8^+$ T cells, and $H\text{-}2D^b\text{-}E7_{49-57}$ T_{RM} cells was observed in *Cxcr6*$^{gfp/gfp}$ mice, when compared with C57BL/6 wild-type mice (figure 5A,B). To reinforce the role of this impaired migration on $CD8^+$ T cells in *Cxcr6*-deficient mice on antitumor immunity, we showed that these specific $CD8^+$ T cells did not exhibit defaults in cytotoxicity mechanisms (online supplemental figure S4).

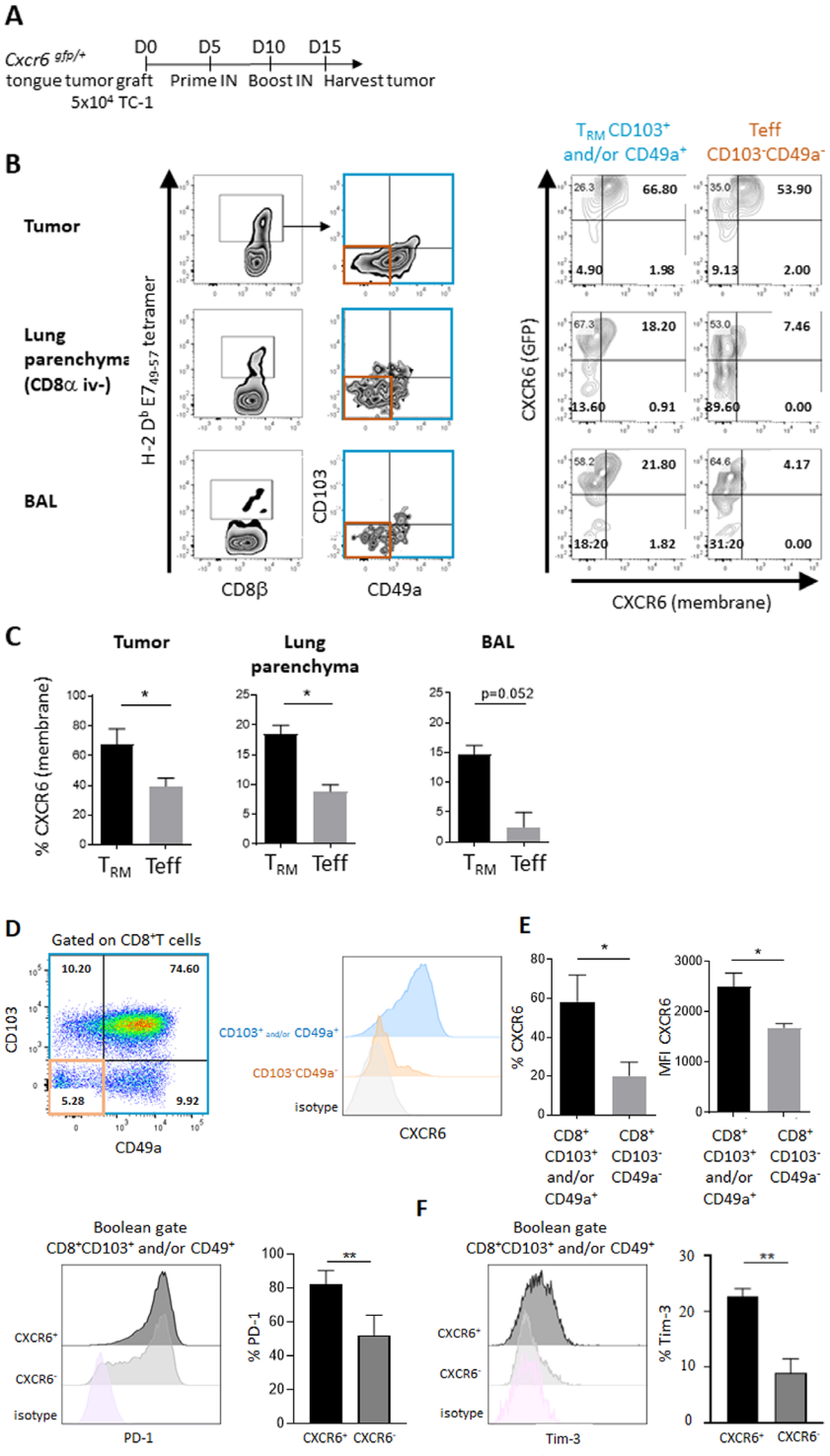

Figure 2 Cxcr6 (membrane expression) is preferentially expressed on CD8$^+$ resident memory T cells in mice and humans. (A) *Cxcr6*$^{gfp/+}$ mice were grafted with TC-1 cells (5×10^4) in the tongue at D0, then vaccinated via the in route with STxB-E7 and poly-ICLC at D5 and D10 and sacrificed at D15. (B) Gating strategy for T_{RM} (in blue: Boolean gate CD103$^+$ and/or CD49a$^+$) and Teff (in orange: CD103$^-$CD49a$^-$). Representative flow plots showing GFP expression versus surface expression of CXCR6 on T_{RM} and Teff. (C) Percentage of CXCR6 membrane expression in tumor, lung parenchyma (CD8a IV$^-$) and BAL. Mean±SEM, n=4/group. Results are representative of two experiments. (D–F) Fresh biopsies from a patient with lung cancer (n=4) were dissociated and digested, and flow cytometry analysis of tumor-infiltrating lymphocytes was then performed. (D) Representative flow plot of CD103 and CD49a expression and gating strategy on live CD8. (E) Representative histograms of CXCR6 expression (left), percentage (middle) and MFI (right) of CXCR6 with T_{RM} phenotype (Boolean gate CD103$^+$ and/or CD49a$^+$) and CD103$^-$CD49a$^-$CD8$^+$ T cells. (F) Representative histograms (left) and percentage of PD1 (right) and Tim-3 (left) among CXCR6$^+$ and CXCR6$^-$ T_{RM}. Mean±SEM paired t-test. Poly-ICLC, polyinosinic-polycytiylic acid-poly-l-lysine carboxymethylcellulose. GFP, Green Fluorescent Protein. *P<0.05, **P<0.01. BAL, bronchoalveolar lavage.

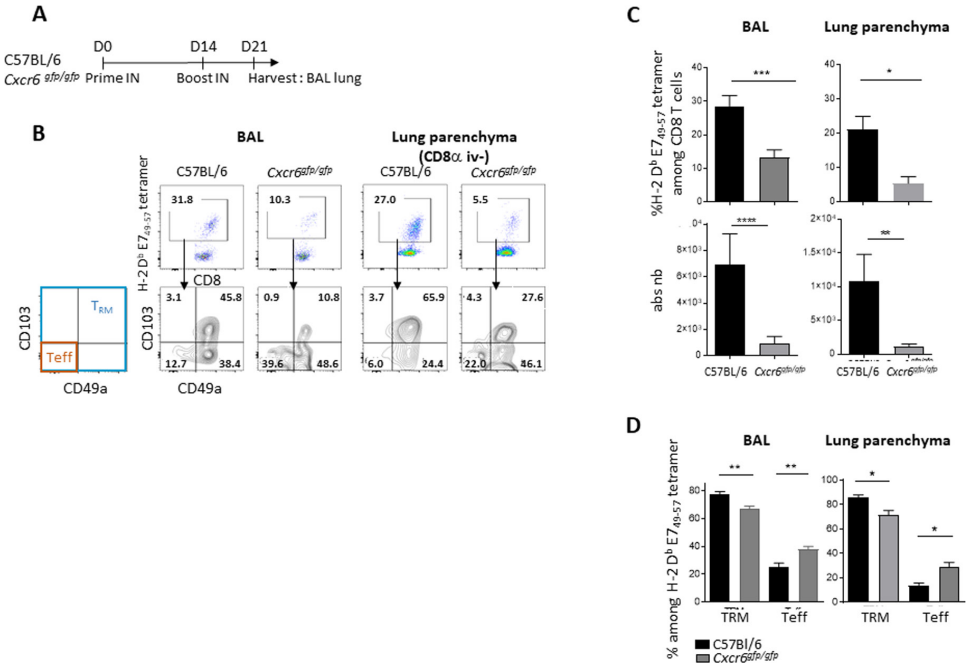

Figure 3 Induction of specific CD8$^+$ T cells and T_{RM} in the lung and airway is impaired in *Cxcr6*-deficient mice (A) C57BL/6 or *Cxcr6*$^{gfg/gfp}$ mice were vaccinated with STxB-E7 via the in route at days 0 and 14, then sacrificed at day 21. (B) Representative flow plots of H-2 D^b $E7_{49-57}$ tetramer gated on CD8$^+$ T cells (top), and T_{RM} (Boolean gate CD103$^+$ and/or CD49a$^+$) and effector T cells (teff) (CD103$^-$CD49a$^-$) in BAL and lung parenchyma gated on H-2 D^b $E7_{49-57}$ tetramer (bottom). (C) Percentage and absolute number of H-2 D^b $E7_{49-57}$ tetramer in BAL and lung parenchyma. (D) Percentage of T_{RM} and teff in BAL (n=21–22 mice/group) and lung parenchyma (n=5–7 mice/group). these experiments were repeated three times. Mean±SEM Mann-Whitney t-test. *P<0.05, **P<0.01, ***P<0.001, ****P<0.0001. BAL, bronchoalveolar lavage.

CXCL16 does not act as a local adjuvant after intranasal vaccination likely due to endogenous production of the chemokine

One of the potential applications of analyzing the role of these chemokine receptors and their ligands is to use them as adjuvants for local homing of CD8$^+$ T cells to the lung. For this purpose, we vaccinated wild-type mice with STxB-E7 in the presence or absence of recombinant CXCL16 during priming and boosting and analyzed the recruitment of specific CD8$^+$ T cells in BAL or lung parenchyma. The addition of recombinant CXCL16 did not show a significant increase in total specific CD8$^+$ T cells nor of those with a T_{RM} phenotype in the BAL (figure 6A) or lung (data not shown). Similar results were observed when recombinant CXCL16 was administered only at prime or boost.

To better understand this observation, we measured the endogenous induction of CXCL16 before and after intranasal vaccination in the BAL and pulmonary parenchyma. We observed an induction of CXCL16 by a factor of 4–5 in the BAL and pulmonary parenchyma with a peak at 48 hours after immunization. Chemokine levels then decline but remain above baseline concentrations for at least 72 hours after vaccination in the lung parenchyma (figure 6C). As other chemokine receptors (CCR5, CXCR3, and CCR6) and their ligands have been implicated in the migration of CD8$^+$ T cells into the lung,[29 37 38] we also measured the induction of these chemokines. In the pulmonary parenchyma, we found an increase in chemokines binding CCR5 (CCL3, CCL4, and CCL5), CCR6 (CCL20), CXCR3 (CXCL10) as early as 24 hours after intranasal vaccination of wild-type mice (online supplemental figure S5). However, in contrast to CXCL16, this induction is transient, and the concentrations of these chemokines return to basal levels within 48–72 hours (online supplemental figure S5). Similar results were found in BAL (data not shown).

Cheek and lung epithelial cells may constitute one source of this production of CXCL16 (online supplemental figure S6). Interestingly, intramuscular immunization with the same vaccine also induces an increase in CXCL16 only in lung parenchyma, but at much lower levels (figure 6C,D) than those observed after intranasal immunization.This high endogenous CXCL16 induction after intranasal vaccination reinforces the physiological role of the CXCL16-CXCR6 axis in the migration of CD8$^+$ T cells to the lung. It may also explain why the intranasal route is more efficient to recruit CD8$^+$ T cells in the lung than the intramuscular route of administration.

DISCUSSION

In this work, we confirmed, at the protein level, that CXCR6 was predominantly expressed on lung T_{RM} as compared with effector CD8$^+$ T cells, whereas memory CD8$^+$ T cells of the spleen did not express this receptor after vaccination.

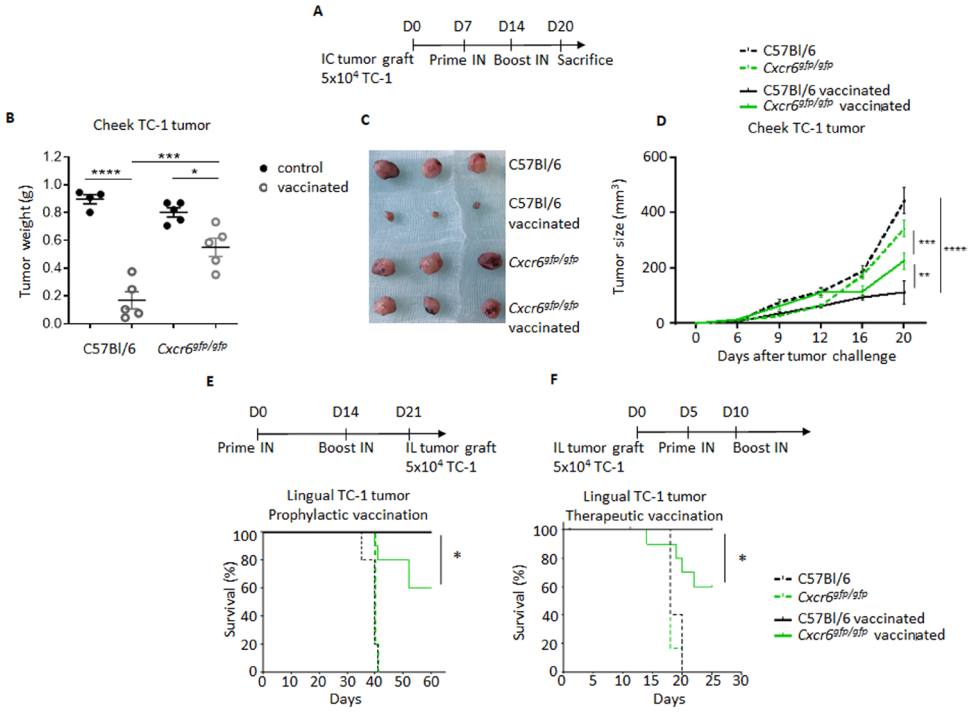

Figure 4 *Cxcr6* deficiency impairs tumor control in orthotopic tumors. (A) C57BL/6 or *Cxcr6*$^{gfg/gfp}$ mice were grafted in the submucosal lining of the cheek (IC) with TC-1 tumor cells, then vaccinated or not with STxB-E7 via the in route at days 7 and 14, and sacrificed at day 20. (B–D) Tumor weight (B,C) and tumor size (D) were measured at day 20. (D,E) In a second orthotopic model, TC-1 was grafted in the sublingual mucosa (IL); mice were then vaccinated following a prophylactic (E) or therapeutic protocol (F), and survival was monitored. All data are representative from two independent experiments. Five mice/group (B–D) and 10 mice/group (E,F). Mean±SEM analysis of within-group differences was performed with a two-way analysis of variance and post hoc Tukey test (B–D), and survival was compared between groups with a Kaplan-Meier curve (log-rank test) (E,F). *P<0.05, **P<0.01, ***P<0.001, ****P<0.0001. IC, intracheek; IL, intralingual.

In addition, we demonstrate for the first time that vaccination of *Cxcr6*-deficient mice causes a defect in recruitment of antigen-specific CD8$^+$ T cells in the lung, especially the T_{RM} subsets. In contrast, this decrease in antigen-specific CD8$^+$ T cells was not observed in CD8$^+$ T cells derived from the spleen of *Cxcr6*-deficient mice. A decrease of total CD8$^+$ T cells in the lung in *CXCR6*-deficient mice has also been reported in infectious models, while the proportion of these cells remained stable in the spleen and bone marrow.[24]

In order to evaluate the consequences of this CD8$^+$ T-cell migration defect in a tumor context, we showed that *Cxcr6*-deficient mice bearing an orthotopic tumor in the head and neck regions are less well protected by an HPV vaccine, after both prophylactic and therapeutic vaccination. The present study is therefore the first to report the direct role of CXCR6 in antitumor immunity.

We have not formally demonstrated that the deficiency of *Cxcr6* in CD8$^+$ T cells directly explains partial loss of cancer vaccine efficacy, as only an inducible *Cxcr6* KO specific to CD8$^+$ T cells, not yet available, would allow specific deletion of these cells. However, the transfer of T cells derived from *Cxcr6*-deficient or wild-type mice confirms the intrinsic role of *Cxcr6* deficiency on T cells in the reduction of T_{RM} in the lung after vaccination by the intranasal route (online supplemental figure S3).

In addition, we have previously shown that this selected TC-1 epithelial tumor model, expressing the HPV E6–E7 protein, is dependent on CD8$^+$ T cells, because in the absence of CD8$^+$ T cells and especially CD8$^+$ resident memory T cells, vaccine efficacy is abolished.[9 10] The present study also demonstrated that the microenvironment of tumors derived from *Cxcr6*-deficient mice and vaccinated with a therapeutic vaccine directed against HPV E7 protein is less intensively infiltrated by total, antigen-specific CD8$^+$ T cells and CD8$^+$ resident memory T cells (figure 5A,B).

CXCR6 does not appear to be involved in the functional activity of CD8$^+$ T cells, because memory CD8$^+$ T cells either expressing or not CXCR6 produce similar levels of cytokines and exhibit equivalent levels of cytotoxicity markers (online supplemental figure S3).[39]

This role of CXCR6 associated with a protective phenotype has also been observed in an infectious model, as when CXCR6-positive and CXCR6-negative CD8$^+$ T cells were isolated and sorted from the lung of mice previously immunized with a vaccine against *Mycobacterium* and injected into naive mice, and challenged with *Mycobacterium tuberculosis*, mice transferred with CXCR6$^+$CD8$^+$ T cells were better protected than mice receiving CXCR6 negative CD8$^+$ T cells.[40]

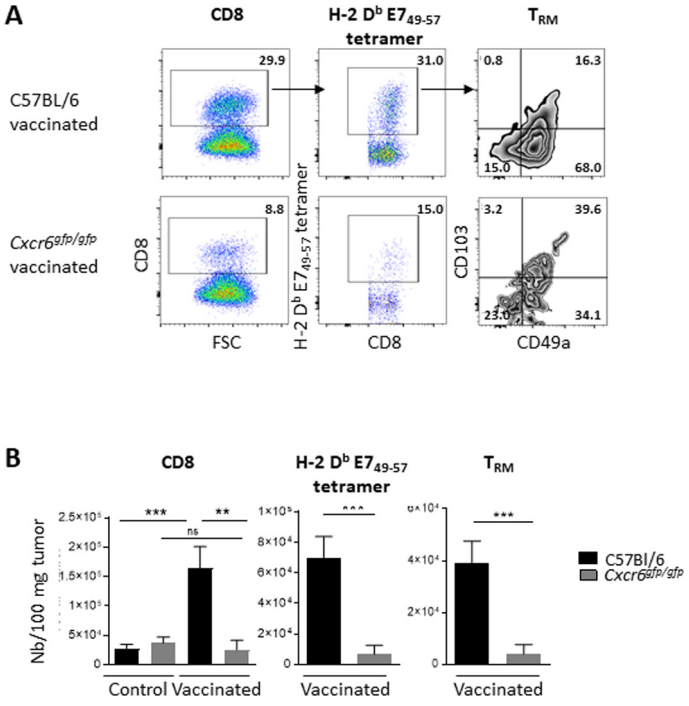

Figure 5 Cxcr6 deficiency impairs CD8$^+$ T-cell infiltration in cheek tumor after in vaccination analysis of CD8 and H-2 D^b E7$_{49-57}$ specific cells infiltrating a TC-1 cheek tumor in C57BL/6 and *Cxcr6$^{gfg/gfp}$* mice, vaccinated or not with STxB-E7 via the intranasal route (D7 and D14) at day 20 after tumor graft. (A) Representative flow plots and (B) total number of CD8 T cells, H-2 D^b E7$_{49-57}$ tetramer and T$_{RM}$ (Boolean gate CD103$^+$ and/or CD49a$^+$). Data are representative of two independent experiments. Five mice/group. Mean±SEM analysis of difference within groups was performed with a one-way analysis of variance and post hoc Tukey test, and between two groups with Mann-Whitney t-test. **P<0.01, ***P<0.001.

The absence of CXCR6 does not totally reverse the effect of the cancer vaccine on controlling tumor growth. Other chemokine receptors have been involved in CD8$^+$ T-cell migration into the lung, as it has been shown that CXCR3 and CCR5 are also important for promoting CD8$^+$ T-cell homing into the lung.[37 38 41] T cells present in BAL fluid of sarcoidosis patients coexpressed CXCR6 and CXCR3.[32] Transcriptomic analyses showed that T$_{RM}$ expressed CXCR6, CCR5, and CXCR3.[29] In our model, in contrast to the sustained induction of CXCL16, we showed a transient increase of CCL3, CCL4, CCL5 and CCL20 chemokines, the respective ligands of these receptors after intranasal vaccination, which could participate in the early recruitment of T cells in the tumor (online supplemental figure S5).

Earlier work by our team has shown that intranasal vaccination induced higher concentrations of antigen-specific CD8$^+$ T cells in the lung or head and neck parenchyma than systemic vaccination.[9 10] The present work demonstrates that these intrapulmonary CD8$^+$ T cells express CXCR6, as already observed in lung derived CD8$^+$ T cells from intranasal immunized mice with recombinant virus.[40 42] The mechanisms explaining this preferential recruitment of CD8$^+$ T cells in the lung and head and neck tumor microenvironment are poorly elucidated. We have shown that lung dendritic cells, rather than spleen derived dendritic cells, can induce an increase of CD49a on CD8$^+$ T cells, which may explain the phenotype of the induced T$_{RM}$ cells but not the migration step.[10] In this work, we report that intranasal vaccination induces a much greater increase in the chemokine CXCL16 in the BAL fluid and lung parenchyma, compared with intramuscular vaccination. This local increase in CXCL16 may explain the preferential recruitment of CXCR6-expressing CD8$^+$ T cells into the lung and the impact of loss of expression of this receptor on CD8$^+$ T-cell migration into the lung. However, we cannot exclude a role of the CXCL16–CXCR6 axis in the persistence of CD8$^+$ T cells in the lung, as already suggested by another study.[21] It has also recently been shown that the CXCR6–CXCL16 axis plays a role in the seeding of airway T$_{RM}$ from lung interstitium.[36 43] While this work and our study show a role for CXCR6 in the recruitment of CD8$^+$ T cells in the lung, other groups did not find an impact of CXCR6 in the pulmonary recruitment of CD4$^+$ T cells after infection.[44]

CXCL16 can be produced by bronchial epithelial cells, dendritic cells, T cells and alveolar macrophages.[15 23] The origin of pulmonary CXCL16 induction after intranasal vaccination remains to be determined. The Demaria group reported that irradiation induced the production of CXCL16 by murine and human tumor lines. Interestingly, in *CXCR6*-deficient mice, irradiation no longer resulted in recruitment of CD8$^+$ T cells.[45]

Nevertheless, the CXCL16–CXCR6 axis is not specific to head and neck or pulmonary tissue because CXCR6 expression has also been demonstrated on iNKT cells in the liver.[19 46] *Cxcr6*-deficient mice have a reduced number of T$_{RM}$ in the skin.[25] One limitation of CAR T cells is their

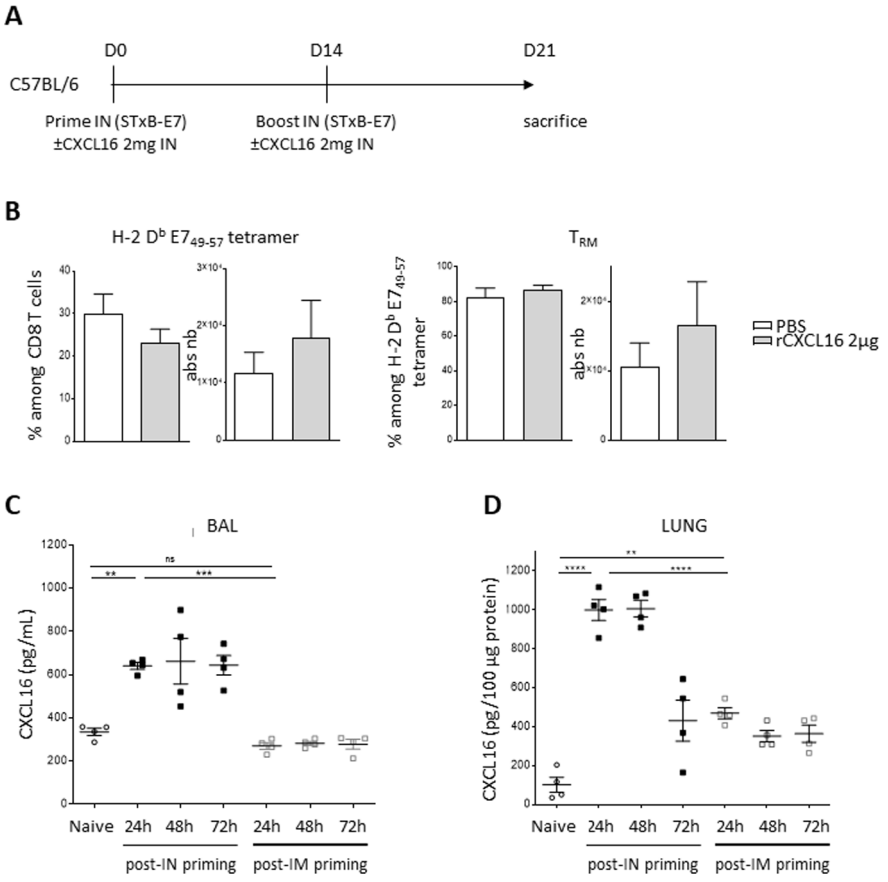

Figure 6 Recombinant CXCL16 did not amplify recruitment of T_{RM} likely due to endogenous CXCL16 induced after vaccination. (A) C57BL/6 mice were vaccinated with STxB-E7 via the in route at days 0 and 14 in the presence or absence of recombinant CXCL16 (2 mg), then sacrificed at day 21. (B) Percentage and absolute number of specific H-2 D^b $E7_{49-57}$ tetramer within CD8 T cells (left) and T_{RM} within tetramer (right) in the BAL are shown. n=8 mice/group. (C,D) C57BL/6 mice were vaccinated with STxB-E7 (20 µg)+poly ICLC (10 µg) via the intranasal or intramuscular route. CXCL16 was measured by ELISA at the indicated times after vaccination in BAL (C) and lysate from the lung (D). n=4 mice/group. The experiments were repeated twice. **P<0.01, ***P<0.001, ****P<0.0001. BAL, bronchoalveolar lavage; ns, not significant.

inefficient homing to solid tumors. The transduction of CXCR6 in CAR T cells could improve their migration into CXCL16 producing solid tumors, such as lung cancers and other tumors (pancreas, head and neck, stomach, ovarian and renal cancers).

Based on our results, CXCL16 could be considered to be an attractive mucosal adjuvant. Presumably because of the high endogenous CXCL16 concentrations, we could not show a role for CXCL16 when combined with an intranasal vaccine (figure 6). Similarly, a prime-pull strategy with a vaccine administered by the intramuscular route and nasal injection of CXCL16 did not significantly improve $CD8^+$ T-cell recruitment (results not shown). Unlike other mucosal sites, local antigen is required for induction of T_{RM} cells in the lungs, which could explain this result.[47]

Induction of T_{RM} in the pulmonary mucosa is an important objective both in oncology to optimize anti-PD-1 therapy in patients with no pre-existing $CD8^+$ T-cell response and in infectious diseases (tuberculosis, influenza, and coronavirus-associated diseases), where these cells have a demonstrated role in the control of infection.[48–51] This work more clearly explains the unique potency of the intranasal route of vaccination to induce these memory T cells in the head and neck and pulmonary mucosa and may participate in improving current cancer vaccine strategies.

Author affiliations
[1]Université de Paris, PARCC, INSERM U970, 75006 Paris, France
[2]Equipe Labellisée Ligue contre le Cancer, Paris, France
[3]Institut Curie, PSL Research University, Cellular and Chemical Biology Unit, U1143 INSERM, UMR3666 CNRS, 75248 Paris Cedex 05, France
[4]INSERM U830, Equipe labellisée LNCC, Siredo Oncology Centre, Institut Curie, 75248 Paris Cedex 05, France
[5]Institut Curie, PSL Research University, Department of Translational Research, 75248 Paris Cedex 05, France
[6]Department of Pathology, APHP, Hôpital Européen Georges Pompidou, 75015 Paris, France
[7]Department of Thoracic Surgery, INSERM UMRS 1138, APHP, Hôpital Europeen Georges Pompidou, 75015 Paris, France
[8]Lung Oncology Unit, APHP, Hôpital Européen Georges Pompidou, 75015 Paris, France
[9]Immunology, APHP,Hôpital Europeen Georges Pompidou, Paris, France
[10]Department of Pathology, APHP, Hôpital Cochin, 75014 Paris, Île-de-France, France
[11]Departement Immunologie, Inflammation et Infection, Institut Cochin, INSERM U1016, CNRS UMR8104, Université de Paris, 75014 Paris, Île-de-France, France
[12]Center of Integrated Protein Science Munich (CIPS-M) and Division of Clinical Pharmacology, Department of Medicine IV, Klinikum der Universität München,

LMU Munich, Germany, Member of the German Center for Lung Research (DZL), Munchen, Germany
[13]German Center for Translational Cancer Research (DKTK), partner site, Munchen, Germany
[14]INSERM UMR 1186, Institut Gustave Roussy, Faculté de Médecine-Université Paris-Sud, Université Paris-Saclay, 94805 Villejuif, France
[15]Unit for Lymphopoiesis, Department of Immunology, Institut Pasteur, INSERM U1223, 75006 Paris, France

Acknowledgements We thank the staff of the European Georges Pompidou Hospital tumor banks (D Geromin and M Largeau) for providing sample materials and the PARCC Histology (C Lesaffre) and cytometry (C Knosp) platform as well as animal facilities (C Suldac and N Perez)

Contributors IG-F, AM, ED, MA, and LP performed experimental work and analyzed and interpreted the data. SK, CB, and TT performed experimental work, analyzed and interpreted the data, and designed the figures. EF, LG, FL-B, CB, DD, and NB contributed to sample collection and analyzed and interpreted the data. NG, CT, ED, SK, and FM-C analyzed and interpreted the data. LJ and RG designed the study and revised the manuscript. TE designed the study, supervised the project, and wrote the manuscript. All authors were involved in the final approval of the manuscript.

Funding This work has been funded by Fondation ARC, INCA PLBio, Labex Immuno-Oncology, Site intégré de recherche en cancérologie (SIRIC CARPEM, SIRIC Curie), Cancéropole d'Ile de France, Carnot Curie Cancer, FONCER. SK is supported by the European Research Council (grant 756017, ARMOR-T).

Competing interests None declared.

Patient consent for publication Not required.

Ethics approval Experimental protocols in mice were approved by Paris Descartes University ethical committee (CEEA 34) in accordance with European guidelines (EC2010/63). The human study was approved by the local ethics committee (CPP Tours. CNRIPH n°18.11.21.67518. 05.03.2019). Informed consent was obtained from all subjects.

Provenance and peer review Not commissioned; externally peer reviewed.

Data availability statement Data are available in a public, open access repository. The data are available upon request from ET (eric.tartouraphp.fr).

ORCID iDs
Emmanuel Donnadieu http://orcid.org/0000-0002-4985-7254
Eric Tartour http://orcid.org/0000-0002-7323-468X

REFERENCES

1 Stolley JM, Johnston TS, Soerens AG, *et al*. Retrograde migration supplies resident memory T cells to lung-draining ln after influenza infection. *J Exp Med* 2020;217:e20192197. doi:10.1084/jem.20192197
2 Fonseca R, Beura LK, Quarnstrom CF, *et al*. Developmental plasticity allows outside-in immune responses by resident memory T cells. *Nat Immunol* 2020;21:412–21.
3 Beura LK, Mitchell JS, Thompson EA, *et al*. Intravital mucosal imaging of CD8$^+$ resident memory T cells shows tissue-autonomous recall responses that amplify secondary memory. *Nat Immunol* 2018;19:173–82.
4 Mami-Chouaib F, Blanc C, Corgnac S, *et al*. Resident memory T cells, critical components in tumor immunology. *J Immunother Cancer* 2018;6:87.
5 Schenkel JM, Masopust D. Tissue-resident memory T cells. *Immunity* 2014;41:886–97.
6 Ganesan A-P, Clarke J, Wood O, *et al*. Tissue-resident memory features are linked to the magnitude of cytotoxic T cell responses in human lung cancer. *Nat Immunol* 2017;18:940–50.
7 Dadi S, Chhangawala S, Whitlock BM, *et al*. Cancer immunosurveillance by tissue-resident innate lymphoid cells and innate-like T cells. *Cell* 2016;164:365–77.
8 Park SL, Buzzai A, Rautela J, *et al*. Tissue-resident memory CD8$^+$ T cells promote melanoma-immune equilibrium in skin. *Nature* 2019;565:366–71.
9 Nizard M, Roussel H, Diniz MO, *et al*. Induction of resident memory T cells enhances the efficacy of cancer vaccine. *Nat Commun* 2017;8:15221.
10 Sandoval F, Terme M, Nizard M, *et al*. Mucosal imprinting of vaccine-induced CD8$^+$ T cells is crucial to inhibit the growth of mucosal tumors. *Sci Transl Med* 2013;5:172ra20.
11 Çuburu N, Graham BS, Buck CB, *et al*. Intravaginal immunization with HPV vectors induces tissue-resident CD8+ T cell responses. *J Clin Invest* 2012;122:4606–20.
12 Sun Y-Y, Peng S, Han L, *et al*. Local HPV recombinant vaccinia boost following priming with an HPV DNA vaccine enhances local HPV-Specific CD8+ T-cell-mediated tumor control in the genital tract. *Clin Cancer Res* 2016;22:657–69.
13 Djenidi F, Adam J, Goubar A, *et al*. CD8+CD103+ tumor-infiltrating lymphocytes are tumor-specific tissue-resident memory T cells and a prognostic factor for survival in lung cancer patients. *J Immunol* 2015;194:3475–86.
14 Blanc C, Hans S, Tran T, *et al*. Targeting resident memory T cells for cancer immunotherapy. *Front Immunol* 2018;9:9.
15 Morgan AJ, Guillen C, Symon FA, *et al*. CXCR6 identifies a putative population of retained human lung T cells characterised by co-expression of activation markers. *Immunobiology* 2008;213:599–608.
16 Kumar BV, Ma W, Miron M, *et al*. Human tissue-resident memory T cells are defined by core transcriptional and functional signatures in lymphoid and mucosal sites. *Cell Rep* 2017;20:2921–34.
17 Mackay LK, Minnich M, Kragten NAM, *et al*. Hobit and Blimp1 instruct a universal transcriptional program of tissue residency in lymphocytes. *Science* 2016;352:459–63.
18 Guo X, Zhang Y, Zheng L, *et al*. Global characterization of T cells in non-small-cell lung cancer by single-cell sequencing. *Nat Med* 2018;24:978–85.
19 Matloubian M, David A, Engel S, *et al*. A transmembrane CXC chemokine is a ligand for HIV-coreceptor Bonzo. *Nat Immunol* 2000;1:298–304.
20 Abel S, Hundhausen C, Mentlein R, *et al*. The transmembrane CXC-chemokine ligand 16 is induced by IFN-gamma and TNF-alpha and shed by the activity of the disintegrin-like metalloproteinase ADAM10. *J Immunol* 2004;172:6362–72.
21 Day C, Patel R, Guillen C, *et al*. The chemokine CXCL16 is highly and constitutively expressed by human bronchial epithelial cells. *Exp Lung Res* 2009;35:272–83.
22 Tabata S, Kadowaki N, Kitawaki T, *et al*. Distribution and kinetics of SR-PSOX/CXCL16 and CXCR6 expression on human dendritic cell subsets and CD4+ T cells. *J Leukoc Biol* 2005;77:777–86.
23 Kim CH, Kunkel EJ, Boisvert J, *et al*. Bonzo/CXCR6 expression defines type 1-polarized T-cell subsets with extralymphoid tissue homing potential. *J Clin Invest* 2001;107:595–601.
24 Heesch K, Raczkowski F, Schumacher V, *et al*. The function of the chemokine receptor CXCR6 in the T cell response of mice against Listeria monocytogenes. *PLoS One* 2014;9:e97701.
25 Zaid A, Hor JL, Christo SN, *et al*. Chemokine receptor-dependent control of skin tissue-resident memory T cell formation. *J Immunol* 2017;199:2451–9.
26 Billerbeck E, Kang Y-H, Walker L, *et al*. Analysis of CD161 expression on human CD8+ T cells defines a distinct functional subset with tissue-homing properties. *Proc Natl Acad Sci U S A* 2010;107:3006–11.
27 Nanki T, Shimaoka T, Hayashida K, *et al*. Pathogenic role of the CXCL16-CXCR6 pathway in rheumatoid arthritis. *Arthritis Rheum* 2005;52:3004–14.
28 Fukumoto N, Shimaoka T, Fujimura H, *et al*. Critical roles of CXC chemokine ligand 16/scavenger receptor that binds phosphatidylserine and oxidized lipoprotein in the pathogenesis of both acute and adoptive transfer experimental autoimmune encephalomyelitis. *J Immunol* 2004;173:1620–7.

29 Hombrink P, Helbig C, Backer RA, *et al*. Programs for the persistence, vigilance and control of human CD8$^+$ lung-resident memory T cells. *Nat Immunol* 2016;17:1467–78.
30 Mackay LK, Rahimpour A, Ma JZ, *et al*. The developmental pathway for CD103(+)CD8+ tissue-resident memory T cells of skin. *Nat Immunol* 2013;14:1294–301.
31 Sowell RT, Goldufsky JW, Rogozinska M, *et al*. Il-15 complexes induce migration of resting memory CD8 T cells into mucosal tissues. *J Immunol* 2017;199:2536–46.
32 Agostini C, Cabrelle A, Calabrese F, *et al*. Role for CXCR6 and its ligand CXCL16 in the pathogenesis of T-cell alveolitis in sarcoidosis. *Am J Respir Crit Care Med* 2005;172:1290–8.
33 Pere H, Montier Y, Bayry J, *et al*. A CCR4 antagonist combined with vaccines induces antigen-specific CD8+ T cells and tumor immunity against self antigens. *Blood* 2011;118:4853–62.
34 Anderson KG, Mayer-Barber K, Sung H, *et al*. Intravascular staining for discrimination of vascular and tissue leukocytes. *Nat Protoc* 2014;9:209–22.
35 Unutmaz D, Xiang W, Sunshine MJ, *et al*. The primate lentiviral receptor Bonzo/STRL33 is coordinately regulated with CCR5 and its expression pattern is conserved between human and mouse. *J Immunol* 2000;165:3284–92.
36 Wein AN, McMaster SR, Takamura S, *et al*. CXCR6 regulates localization of tissue-resident memory CD8 T cells to the airways. *J Exp Med* 2019;216:2748–62.
37 Jeyanathan M, Afkhami S, Khera A, *et al*. Cxcr3 signaling is required for restricted homing of parenteral tuberculosis vaccine-induced T cells to both the lung parenchyma and airway. *J Immunol* 2017;199:2555–69.
38 Kohlmeier JE, Miller SC, Smith J, *et al*. The chemokine receptor CCR5 plays a key role in the early memory CD8+ T cell response to respiratory virus infections. *Immunity* 2008;29:101–13.
39 Tse S-W, Radtke AJ, Espinosa DA, *et al*. The chemokine receptor CXCR6 is required for the maintenance of liver memory CD8$^+$ T cells specific for infectious pathogens. *J Infect Dis* 2014;210:1508–16.
40 Lee LN, Ronan EO, de Lara C, *et al*. CXCR6 is a marker for protective antigen-specific cells in the lungs after intranasal immunization against Mycobacterium tuberculosis. *Infect Immun* 2011;79:3328–37.
41 Kohlmeier JE, Reiley WW, Perona-Wright G, *et al*. Inflammatory chemokine receptors regulate CD8(+) T cell contraction and memory generation following infection. *J Exp Med* 2011;208:1621–34.
42 Jiang JQ, He X-S, Feng N, *et al*. Qualitative and quantitative characteristics of rotavirus-specific CD8 T cells vary depending on the route of infection. *J Virol* 2008;82:6812–9.
43 Takamura S, Kato S, Motozono C, *et al*. Interstitial-resident memory CD8$^+$ T cells sustain frontline epithelial memory in the lung. *J Exp Med* 2019;216:2736–47.
44 Ashhurst AS, Flórido M, Lin LCW, *et al*. CXCR6-Deficiency Improves the Control of Pulmonary *Mycobacterium tuberculosis* and Influenza Infection Independent of T-Lymphocyte Recruitment to the Lungs. *Front Immunol* 2019;10:339.
45 Matsumura S, Wang B, Kawashima N, *et al*. Radiation-induced CXCL16 release by breast cancer cells attracts effector T cells. *J Immunol* 2008;181:3099–107.
46 Geissmann F, Cameron TO, Sidobre S, *et al*. Intravascular immune surveillance by CXCR6+ NKT cells patrolling liver sinusoids. *PLoS Biol* 2005;3:e113.
47 Takamura S, Yagi H, Hakata Y, *et al*. Specific niches for lung-resident memory CD8+ T cells at the site of tissue regeneration enable CD69-independent maintenance. *J Exp Med* 2016;213:3057–73.
48 Hu-Lieskovan S, Lisberg A, Zaretsky JM, *et al*. Tumor characteristics associated with benefit from pembrolizumab in advanced non-small cell lung cancer. *Clin Cancer Res* 2019;25:5061–8.
49 Schmidt ME, Varga SM. The CD8 T cell response to respiratory virus infections. *Front Immunol* 2018;9:678.
50 Stary G, Olive A, Radovic-Moreno AF, *et al*. Vaccines. A mucosal vaccine against Chlamydia trachomatis generates two waves of protective memory T cells. *Science* 2015;348:aaa8205.
51 Edwards J, Wilmott JS, Madore J, *et al*. CD103$^+$ Tumor-Resident CD8$^+$ T Cells Are Associated with Improved Survival in Immunotherapy-Naïve Melanoma Patients and Expand Significantly During Anti-PD-1 Treatment. *Clin Cancer Res* 2018;24:3036–45.

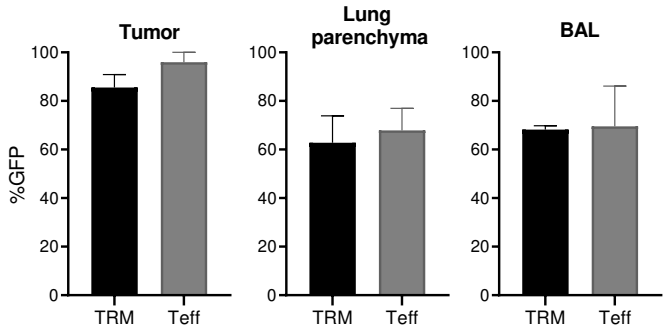

Fig S1: Percentage of GFP (surrogate of CXCR6 transcriptional expression) on T_{RM} and effector T cells in *Cxcr6* $^{gfp/+}$ after IN vaccination.
Cxcr6 $^{gfp/+}$ mice (n = 4) were grafted with TC-1 cells ($5x10^4$) in the tongue at D0, then vaccinated by IN route with STxB-E7 and poly-ICLC at D5 and D10, and sacrificed at D15. GFP expression on T_{RM} and effector $CD8^+$ T cells (Teff) was analyzed by flow cytometry in the tumor, lung parenchyma (CD8a iv-) and BAL (n=3 mice/group). Results are representative of two experiments. Mean ±sem is shown.*P < 0.05; ** P < 0.01

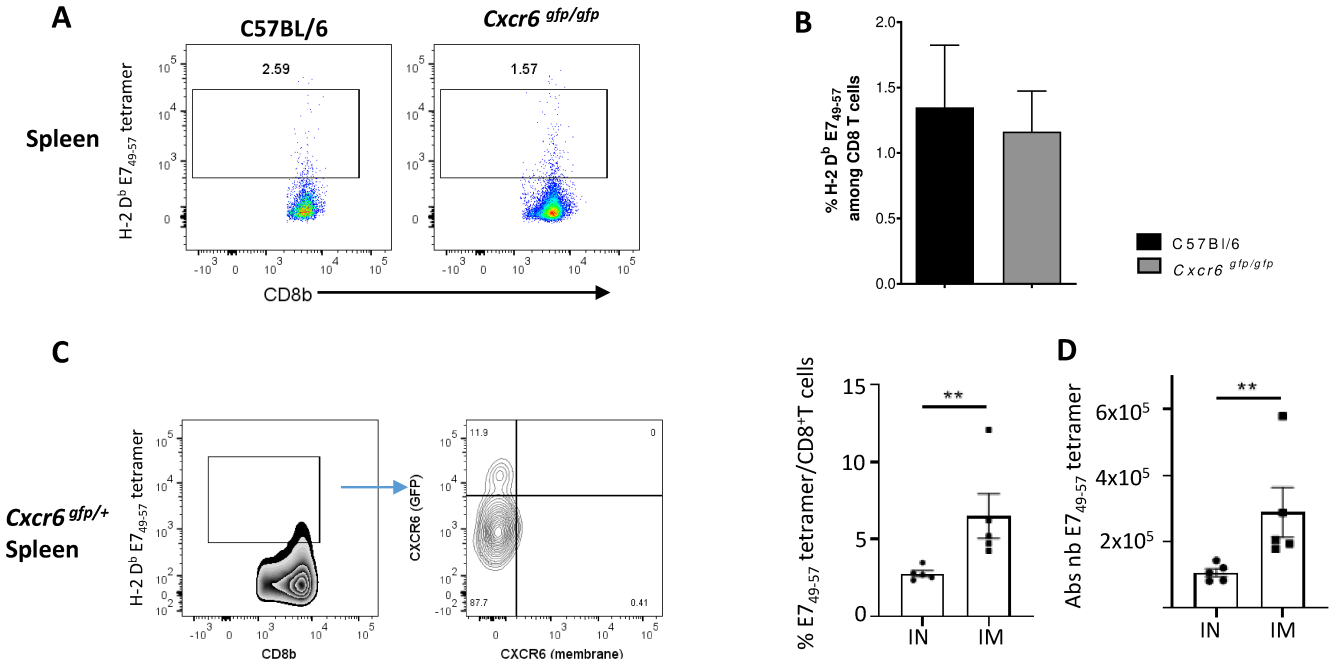

Fig S2*: Cxcr6*$^{gfp/gfp}$ and C57BL/6 mice have similar levels of H-2D^b E7 tetramer in the spleen after IN vaccination

(A-B) C57BL/6 or *Cxcr6*$^{gfg/gfp}$ mice were vaccinated with STxB-E7 by IN route at day 0 and 14, then sacrificed at day 21. Representative flow plots (A) and percentage of specific H-2D^b E7 tetramer gated on CD8$^+$ T cells (B) in the spleen. Mean ±sem. n=16 mice/group.

(C) *Cxcr6* $^{gfp/+}$ mice were grafted with TC-1 cells (5x10^4) in the tongue at D0, then vaccinated via the IN route with STxB-E7 and poly-ICLC at D5 and D10, and mice were sacrificed at D15. Representative flow plots showing expression of CXCR6 (GFP and surface) among H-2D^b E7 tetramer in the spleen. D : C57BL/6 mice (n = 5) were immunized with STxB-E7 by IN or IM route at day 0 and 14, then sacrified at day 21. Percentage and absolute number are shown.

n=5 mice/group. Mean ±sem. Mann-Whitney t-test *p<0.05 **p<0.01

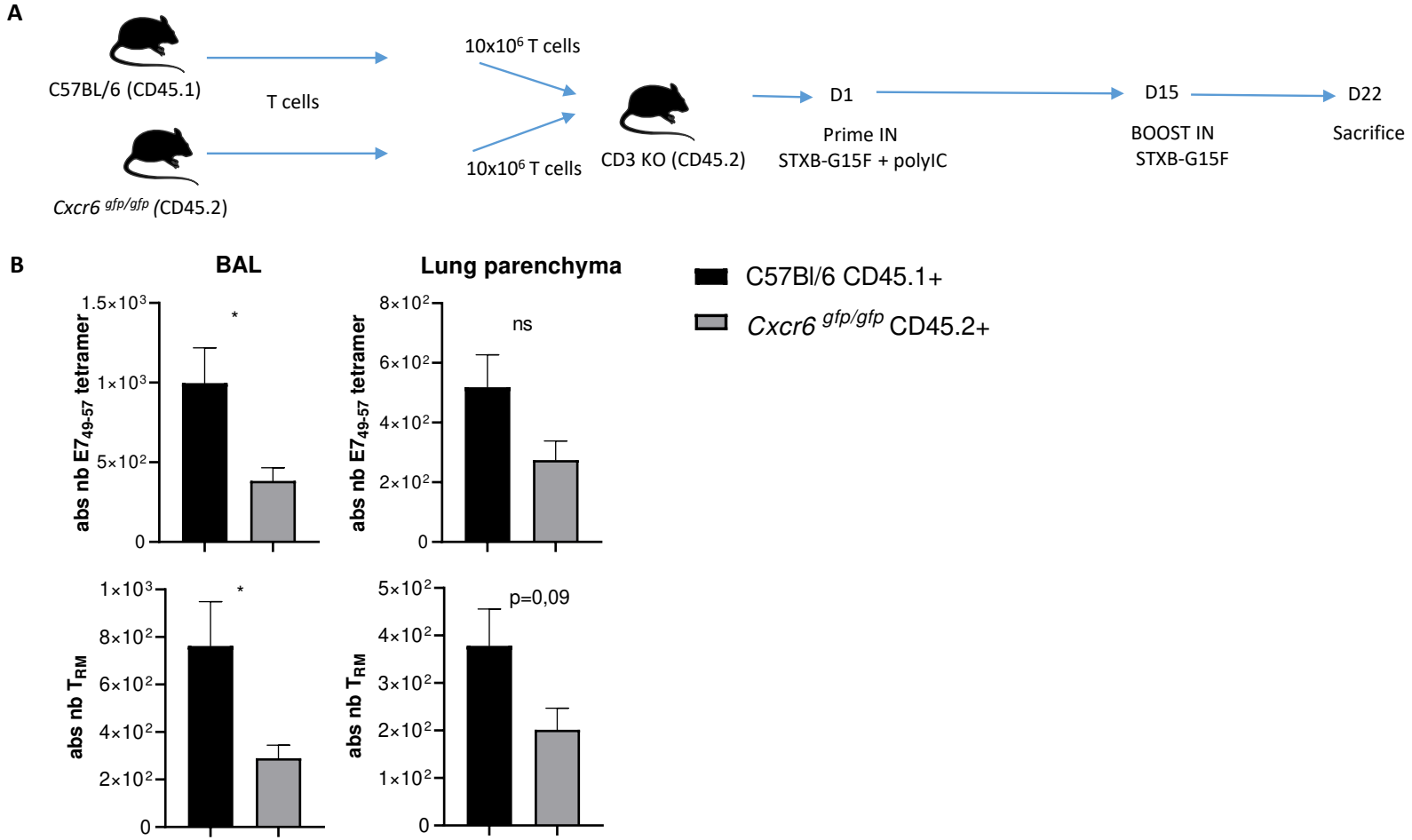

Fig S3 : Role of CXCR6 on T cells in the decrease number of specific CD8⁺T_{RM} in the lung.

A : Description of the experimental design of competitive adoptive transfer of T cells derived from CXCR6 deficient or non-deficient mice congenic for CD45

B : T cells isolated from spleen of naive C57BL/6 (CD45.1) and *Cxcr6* $^{gfp/gfp}$ (CD45.2) were expanded *in vitro* on anti-CD3 coated plates + IL-2 (4ng/ml) for 5 days in RPMI complete medium, then incubated an additional 2 days in the presence of IL-2 (2 ng/ml).

In vitro activated T cells were harvested, washed, mixed at equal numbers in PBS, then injected i.v into CD3 KO recipient mice which were then immunized with STxB-E7 by IN route at day 1 and 21 and sacrified at day 28. Absolute number of H-2D^b $E7_{49-57}$ tetramer and specific T_{RM} were analyzed in BAL and lung parenchyma.

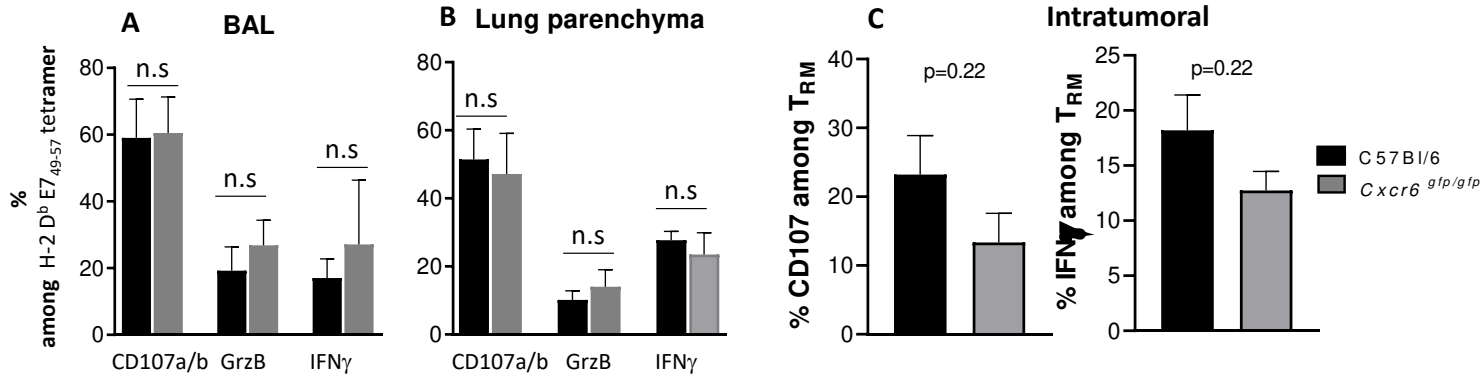

Figure S4: *Cxcr6* deficiency does not impair the functionality of antigen-specific CD8⁺ T cells

A-B : C57Bl/6 and *Cxcr6*$^{gfg/gfp}$ mice were vaccinated with STxB-E7 via the IN route at day 0 and 14, then sacrificed at day 21. C : C57BL/6 or *Cxcr6* $^{gfp/gfp}$ mice were grafted in the submucosal lining cheek (IC: intra-cheek) with TC-1 tumor cells, then vaccinated with STxB-E7 by IN route at day 7 and 14, and sacrified at day 20. Lymphocytes from BAL (A) , lung parenchyma (B) or from the tumor after cell dissociation (C) were stimulated with the $E7_{49-57}$ peptide (10 µg/mL)(A, B) or the TC1 tumor for 5h, in the presence of anti-CD107a/b antibody, Golgistop® (monensin) and Golgiplug® (Brefeldin A). Percentages of CD107a/b, GrzB and IFNγ among $E7_{49-57}$ tetramer in BAL (A) and lung parenchyma (B) or E7 spéoific T_{RM} (C) were analyzed by flow cytometry.

Mean ±sem. n=3-5 mice/group. Data are representative of 2 independent experiments. n.s = not significant

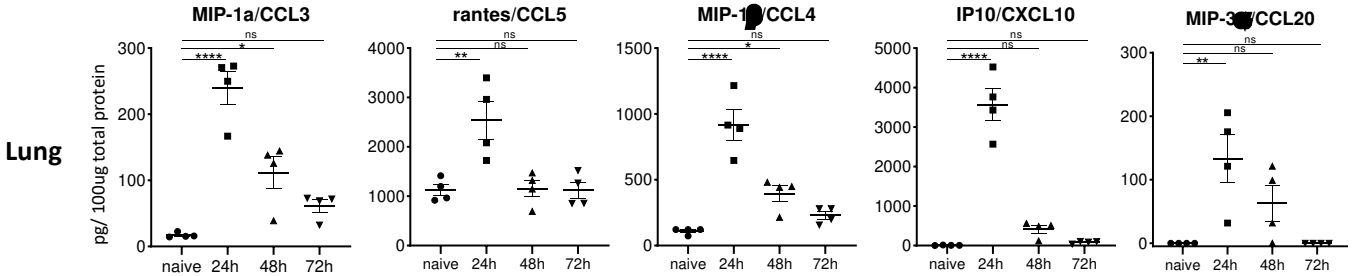

Figure S5 : Other chemokines are transiently modulated after IN vaccination.

C: C57BL/6 mice were vaccinated intranasally with STxB-E7 (20 µg)+poly-ICLC (10 µg). Chemokines CCL3, CCL5, CCL4, CXCL10 and CCL20 were measured by Luminex assay in lysate from lung at the indicated times after immunization. Data are representative of 2 independent experiments with 4 mice/group. Mean ±sem. Mann-Whitney t-test. *P < 0.05; ** P < 0.01; *** P < 0.001; ****P < 0.0001

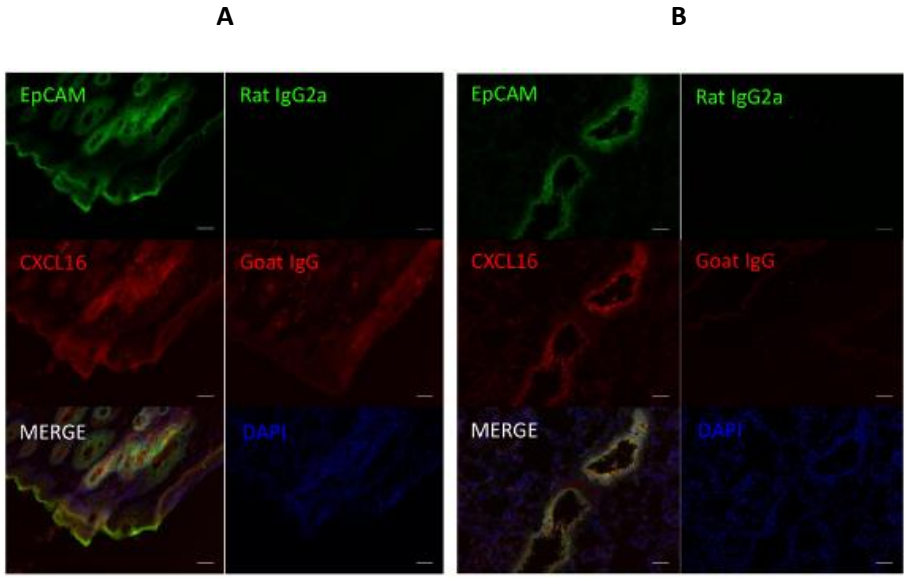

Fig S6 : CXCL16 is expressed by epithelial cells derived from the mucosal lining cheek and lung.

Frozen section from mucosal lining cheek (A) and lung (B) derived from mice previously injected with Poly:IC were stained with antibodies against epithelial cells (Epcam) or CXCL16. Isotype control antibodies were included in each experiment. Nuclei were highlighted using DAPI solution (1ug/mL, Sigma D9542), slides were mounted with mounting medium (DAKO, S3023). Images were acquired x20 on Vectra® 3 automated microscope and analyzed with inForm® Image Analysis Software. Scale bars are 50 μm.

Supplemental materiel and method

***In vitro* stimulation and intracellular cytokine staining**

Lymphocytes from BAL , parenchyma lung or cheek tumor were harvested at D21. Cells were stimulated or not with 10 ug/ml R9F peptide or TC1 tumor cells for 5h in the presence of Golgistop® (Monensin) and Golgiplug® (Brefeldin A), and anti-mouse CD107a/CD107b (clone 14DB and M3/84) (all from BS Biosciences). Then cells were stained with antibodies to surface markers as described above, fixed and permeabilized using Fixation/permeabilization kit (Ebiosciences/Life Technologies) according to manufactor's protocol. And stained for intracellular with antibodies against IFNγ BV650 (XMG1.2, Biolegend) and GranzymeB AF700 (clone GB11, Biolegend).

Immunofluorescence microscopy

C57BL/6 mice were injected i.n with PolyIC (10ug). 24h later, 250ug Brefeldin A (Sigma, B6542) were injected i.v 4h before sacrifice. Intracardiac perfusion with 20ml PBS-EDTA 2mM followed with 10 ml PBS-OCT 2% were performed on anesthezied mice. Lung, mucosal lining cheek were harvested, embedded in Tissue Freezing Medium (Microm Microtech, TFM-5) frozen and stored at -80°C. Blocks were sectioned at 6um with a cryostat, air dried and fixed for 3 min with 100% acetone. Before incubation with antibodies, the slides were pretreated with avidin/biotin blocker (Vector Laboratories SP-2001) for 10 minutes each, and slides were blocked again with 100uL with PBS-BSA 5%+ 0,25% blocking reagent (Perkin Elmer, FP1020) for 30 minutes. Slides were stained with a goat IgG anti-human CXCL16 biotin (2ug/ml, R&D BAF503) or negative control Goat IgG (2ug/mL, R&D BAF108), wash, then stained with Streptavidine -Cy3 (4,5ug/mL, JIR 016-160-084) and rat IgG2a anti EpCAM AF594 (2,5ug/mL, clone G8.8 Biolegend 118222) or control rat IgG2a AF594 (2,5ug/mL, Biolegend 400555). Nuclei were highlighted using DAPI solution (1ug/mL, Sigma D9542), slides were mounted with mounting medium (DAKO, S3023). Images were acquired x20 on Vectra® 3 automated microscope (Akoya/Perkin Elmer) and analyzed with inForm® Image Analysis Software.

Adoptive transfer of T cells

Splenic CD4 and CD8 T cells from C57Bl/6 CD45.1 and *Cxcr6*$^{gfp/gfp}$ mice were isolated by magnetic sorting (Miltenyi Biotec). Then stimulated in vitro with coated anti-CD3ε (clone 145-2C11, Ebioscience/ Life Technologies) with complete RPMI 1640 medium and mouse IL-2 (4ng/ml, PeproTech) for 5 days. T cells were moved into uncoated wells and cultured in complete RPMI 1640 medium and 2ng/ml IL-2 for an additional 2 days. Activated T cells were

washed and cell viability was determined. Equal number of T cells were mixed and injected into CD3 KO recipient mice. Recipient mice were immunized with STxB-E7 by IN route at day 1 and 21 after adoptif transfert, and sacrified at day 28. H-2D^{b} E7$_{49\text{-}57}$ tetramer and T_{RM} were analyzed in BAL and lung parenchyma.